Ejection Dynamics and Electronic Processes Governing Secondary Particle Emission in SIMS

P. Terrence Murray and J. Wayne Rabalais*

Contribution from the Department of Chemistry, University of Houston, Houston, Texas 77004.
Received May 19, 1980

Abstract: A qualitative model for secondary particle emission from simple materials based on the ejection dynamics and electronic charge exchange processes occurring during sputtering is developed and applied to the interpretation of specific cluster types observed in secondary ion mass spectrometry (SIMS). The model considers that a large amount of energy is deposited at a localized site as a result of a collision of a single primary ion to produce a transient localized activated region in the selvedge. The origins of final secondary particles emitted from this selvedge are traced to three dynamical processes: (i) nonreactive ejection, (ii) rearrangement and attachment reactions in the selvedge, and (iii) fragmentation of clusters. The final charge states of these particles, which are largely determined by resonance and Auger electronic charge-exchange transitions between the surface and particle while the two are separated by only a few angstroms, are related to the band structure of the solid and the discrete energy levels of the secondary particles. The model is applied to the interpretation of SIMS data for four basic types of materials with specific examples of each type: (a) metals–metal oxides (Al–Al_2O_3), (b) semiconductors (Si–SiO_2), (c) ionic solids (NaCl), and (d) molecular solids (ice, formic acid, and $Ni(CO)_4$ at 77 K). Qualitative agreement is obtained between the predictions of the model and the relative intensities of specific positive and negative secondary ions observed in SIMS.

I. Introduction

Secondary ion mass spectrometry (SIMS) is establishing a place for itself among surface analytical techniques[1] largely due to its extreme sensitivity[2,3] (10^{-6} monolayer for many metals and some molecules), the detectability of all elements as well as isotopic and isomer sensitivity,[4] the ability to access working surfaces[5] such as catalysts and electronic devices, the sensitivity to molecular and crystal structure in the outer 2–3 atomic layers of a material,[6-8] and the ability to ionize and detect large involatile and thermally fragile molecules deposited on metal surfaces[9-11] and matrix isolated organic species.[12] Basic to a complete understanding of SIMS of materials is the elucidation of the mechanism by which specific secondary atomic and molecular species are produced in various charge states (positive, neutral, or negative) during primary ion bombardment. We have recently[13-15] proposed a general qualitative clustering mechanism which is consistent with the molecular ion clusters observed in SIMS of rather diverse materials. This mechanism involves transient thermal activation of a localized site by a single primary ion impact followed by irreversible expansion to relieve the nonequilibrium situation. Bound clusters consisting of atoms from contiguous as well as noncontiguous lattice sites are ejected from the selvedge region during this expansion.

The ejection dynamics and electronic transitions that can occur near a surface govern the types of clusters and their relative intensities observed in SIMS. The purpose of this paper is to provide a model which outlines the origins of sputtered particles and the electronic processes that are operative as secondary particles leave a surface and to present the SIMS of materials that exemplify these processes. The model is necessarily qualitative and empirical, for many of the details of the processes involved are active areas of research which are still incompletely understood. Nevertheless, it is capable of predicting and providing an understanding of the extreme variations in secondary ion abundances which are ubiquitous to SIMS of even the simplest materials; this is the facet wherein its importance lies. The paper is organized as follows. Section II details the origins of secondary particles into two categories: (A) the dynamics of secondary particle production, i.e., the methods by which specific atoms become arranged into a cluster, and (B) the particle–surface electronic charge-exchange and excitation processes that control the final charge state and stability of the clusters. The experimental procedures for obtaining the SIMS are presented in section III. The SIMS results, presented in section IV, are grouped into four major categories: (A) metals–metal oxides, (B) semiconductors, (C) ionic solids, and (D) molecular solids (spectra representative of each major group are discussed). The examples used include new SIMS data as well as some previously published SIMS. The paper is concluded in section V with a consideration of the generality of the theoretical model, and its ability to predict and interpret specific features in SIMS.

II. Origins of Secondary Particles

A. Dynamics of Secondary Particle Production. Energetic primary ions undergoing elastic and inelastic surface collisions can transfer their momentum in collision cascades to lattice atoms in the vicinity of a collision site. At the primary ion fluxes normally employed in SIMS (10^{-6}–10^{-9} A/cm^2), the time interval between primary ion arrivals at surface sites (even those as large as ~50-Å radius) is greater than a few seconds. Since this is many orders of magnitude longer than the time required to dissipate the momentum of the primary ion and for the secondary ions to leave the surface, all secondary particles are produced by the collision of a single primary ion; multiple primary ion events are insignificant. The primary ion momentum is transferred to lattice atoms as the cascades propagate in random directions, such a process requiring only $\sim 10^{-13}$ s or less.[16] The nonequilibrium situation induced by depositing a large amount of energy almost

(1) R. J. Day, S. E. Unger, and R. G. Cooks, *Anal. Chem.*, **52**, 557A (1980).
(2) R. W. Hewitt, A. T. Shepard, W. E. Baitinger, and N. Winograd, *Anal. Chem.*, **50**, 1286 (1978).
(3) R. J. Colton, J. S. Murday, J. R. Wyatt, and J. J. DeCorpo, *Surf. Sci.*, **84**, 235 (1979).
(4) F. Honda, Y. Fukuda, and J. W. Rabalais, *Chem. Phys.* **47**, 59 (1980).
(5) E. J. Fasiska and P. B. Janocko, *Proc. Annu. Conf.-Microbeam Anal. Soc.*, 76A (1977).
(6) P. H. Dawson and W. C. Tam, *Surf. Sci.*, **81**, 464 (1979); **81**, 164 (1979); P. H. Dawson, *ibid.*, **57**, 229 (1976); **65**, 41 (1977).
(7) H. Hopster and C. R. Brundle, *J. Vac. Sci. Technol.*, **16**, 548 (1979).
(8) T. Fleisch, N. Winograd, and W. N. Delgass, *Surf. Sci.*, **78**, 141 (1978).
(9) R. J. Day, S. E. Unger, and R. G. Cooks, *J. Am. Chem. Soc.*, **101**, 501 (1979); *Anal. Chem.*, **52**, 353 (1980).
(10) A. Benninghoven and W. Sichterman, *Org. Mass Spectrom.*, **12**, 1180 (1978).
(11) H. Grade, N. Winograd, and R. G. Cooks, *J. Am. Chem. Soc.*, **99**, 7725 (1977).
(12) H. T. Jonkman, J. Michl, R. N. King, and J. D. Andrade, *Anal. Chem.*, **50**, 2078 (1978).
(13) F. Honda, G. M. Lancaster, Y. Fukuda, and J. W. Rabalais, *J. Chem. Phys.*, **69**, 4931 (1978).
(14) G. M. Lancaster, F. Honda, Y. Fukuda, and J. W. Rabalais, *J. Am. Chem. Soc.*, **101**, 1951 (1979).
(15) F. Honda, Y. Fukuda, and J. W. Rabalais, *J. Chem. Phys.*, **70**, 4834 (1979).
(16) J. N. Coles, *Surf. Sci.*, **79**, 549 (1979).

0002-7863/81/1503-1007$01.25/0

instantaneously into a localized region can be relieved by an irreversible expansion[14] into the vacuum. The random motion acquired by the lattice atoms in this region can propagate them out of the surface into the vacuum if their velocity vectors are in the appropriate direction and sufficiently large to overcome the surface binding energy. This localized high-energy region can be considered[16] a transient high-density plasma in the selvedge (the interface region between the solid and gas phases) where reactions can occur. Particles propagating through the selvedge can combine to form large clusters if they are so synchronized in space, time, and velocity such that the attractive potential energy, V, between them is greater than the differences in their relative kinetic energies, E^k, that is[13,14]

$$(E^k + V) < 0 \qquad (1)$$

and if they can undergo stabilizing collisions. Such a process has been shown[15] to account for the fact that secondary molecular ions can be ejected as single entities whose constituent atoms result from contiguous lattice sites, or they can be ejected as rearranged species whose constituent atoms originate from both adjacent and nonadjacent lattice sites due to reactions in the selvedge. Such clusters can undergo a unimolecular decomposition during their flight from the selvedge to the detector. This process has been modeled by dynamical calculations of the classical ion trajectories in sputtering where it has been shown[17] that rearrangement and association reactions just above the surface are responsible for production of many of the clusters observed in SIMS.

From the mechanism outlined above, it is evident that the origins of sputtered particles can be traced to three distinct processes: (i) nonreactive ejection, (ii) reactions in the selvedge, and (iii) fragmentation of clusters. These three processes are detailed below.

(i) **Nonreactive Ejection.** Nonreactive ejection is the process by which the momentum of the primary ion that is transferred to the lattice initiates atomic motion which has a component of momentum directed out of the surface such that an atom, molecule, or molecular fragment (either neutral or charged) is ejected from the surface without undergoing any recombination with other particles. Since the energy content per unit volume in the collision site is extremely high (sufficient to atomize a material), most entities sputtered by this process will originate from the periphery of the activated region where the energy content is somewhat lower. Such particles typically[13,14,18] have kinetic energy distributions which are broad and peak higher than particles from the other processes due to the lack of other channels for dissipating their energy. The chemical environment at a surface is, therefore, reflected in the elemental composition of such particles.

(ii) **Reactions in the Selvedge.** Reactions[15] occurring between the ions, atoms, molecules, and molecular fragments in the selvedge can form clusters which contain atoms from nonadjacent lattice sites. Since the effective transient temperature of the activated region is comparable[16] with particle velocities of the order 10^6–10^7 cm/s and since the density of these particles is very high (similar to the atomic density of the crystal) resulting in a short mean free path,[14,16] encounters of the type described in eq 1 can occur at a rate of $\sim 10^{-14}$ s^{-1}. Under these conditions clusters can result which contain a considerably different atomic composition than expected from the surface structure. The dominant cluster types ejected are those that represent the highest thermodynamic stability in the elementary reactions and attachment processes occurring in the environment.

(iii) **Fragmentation of Clusters.** Molecular clusters formed by either of the above-mentioned processes can undergo unimolecular dissociation. Considering the average secondary ion energies and the path length through the mass spectrometer, it has been shown[13] that clusters must have a minimum lifetime of the order of tenths of milliseconds in order to reach the detector. The observation[14] of large clusters (with up to 154 atoms) and doubly charged molecular ions (where strong Coulombic repulsions are prevalent) in SIMS suggests that a significant fraction of molecular clusters have sufficiently low internal energies and, therefore, long lifetimes, such that they can be detected.

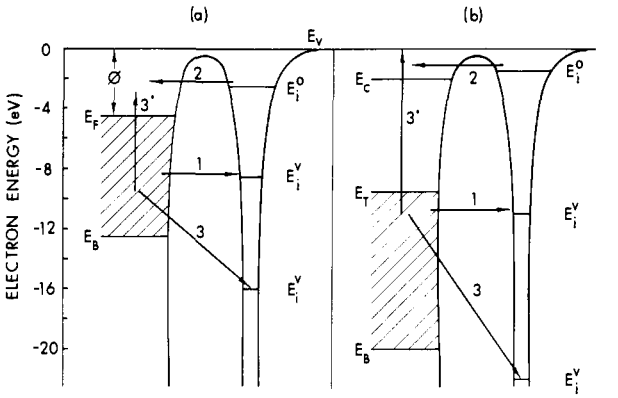

Figure 1. Electron energy diagrams representing a secondary particle departing a surface during the sputtering event. The electronic band structures of typical (a) metallic and (b) insulating surfaces are shown along with discrete energy levels of neutrals or ions in their potential wells. The abscissa represents the distance from the surface to the departing particle, and the ordinate represents the energy of an electron in the solid or particle. The filled valence band is shown shaded. The most probable charge-transfer electronic transitions that can occur between the particle and the surface while the departing particle is within angstroms of the surface are indicated. Transition 1 represents a resonance surface-to-particle (S → P) transition from the valence band to a vacant level, E_i^V, of the particle, e.g., resonance neutralization of a departing positive ion into an excited level or ground state of the neutral species. A resonance particle-to-surface (P → S) transition from an occupied level, E_i^0, of the particle into the conduction band is indicated by transition 2, e.g., resonance neutralization of a departing negative ion into an excited level or ground state of the neutral species. Transitions 3 and 3′ represent a two-electron Auger process in which a valence band electron tunnels into a particle vacancy at E_i^V and the energy gained is transferred to another valence band electron which can be excited into the conduction band or ejected into the continuum, e.g., Auger neutralization of a departing positive ion.

B. Electronic Processes Determining the Final Charge State of Secondary Particles. After a secondary particle has been formed through one of the above-mentioned pathways, its electronic charge state may be altered by electron-exchange processes between the secondary particle and surface; the type of exchange process and the final charge state of the particle are determined by the electronic energy levels of the solid and those of the secondary particle. In the category of fast, and therefore important, electronic transitions between a particle and a surface, two processes dominate:[19] (i) *adiabatic or resonance tunneling processes* and (ii) *two-electron or Auger transitions*. These processes are illustrated by electron energy diagrams in Figure 1 for typical metallic and insulating surfaces, respectively. In Figure 1a the Fermi level, E_F, of the metal lies below the vacuum level, E_V, by an energy interval equal to the work function, ϕ, and the width of the filled levels is from E_F to the bottom of the valence band, E_B. Typical energy levels of the atom, ion, or molecular species leaving the surface are drawn inside the potential well of the free particle at the right of the surface structure. For an insulating surface (Figure 1b), E_C represents the bottom of the conduction band, E_T and E_B represent the top and bottom, respectively, of the valence band, and $E_T - E_C$ is the band gap or forbidden region between the valence and conduction bands. The exact details of the valence band structure are not critical to this qualitative model; naturally, electron transfer from the solid will have the highest probability at energies corresponding to a high density of occupied valence band states. The energy levels of the atomic or molecular species are broadened near the surface due to the interaction of the particle

(17) B. J. Garrison, N. Winograd, and D. E. Harrison, Jr., *J. Chem. Phys.*, **69**, 1440 (1978).
(18) K. Wittmaack, *Inelastic Ion-Surface Collisions* [*Int. Workshop*], 153 (1977).
(19) H. D. Hagstrum, *NATO Adv. Study Insti. Ser., Ser. B*, **32**, 273 (1978).

with the surface. The most significant interactions[20,21] are (i) the Coulombic image force of attraction for ions, (ii) the dynamical effects on changing the relative energies of levels in the solid and particle, and (iii) electronic repulsions arising from interpenetrating electron clouds and the Pauli principle. Interaction (i) is normally dominant[20] for the low-energy particles considered herein. This interaction is brought about when a charged particle moving near a surface induces polarization of the electronic structure of the material, thus producing a Coulombic image force of attraction which shifts the ionization potentials of the particle. This image potential has been shown[20] to follow the expression $-e^2/4s$ (modified by the dielectric constant for insulators), where s is the particle–surface distance. For a singly charged ion, this image potential is typically[21,22] of the order of 0.4 eV at 5 Å from the surface rising to ~1 eV at 2 Å and can induce comparable reductions in the energy levels of the particle. However, increases in these energy levels of a comparable order can be expected due to relaxation energy between the ion and neutral species. Obviously, some cancellation of these two effects can be expected, although together they contribute uncertainty in the exact positions of the energy levels of emerging particles. Such perturbations are within the qualitative realm of this model.

Electronic transitions[19-22] that can alter the charge state of a secondary particle as it departs a surface are indicated by the arrows in Figure 1. These transitions are detailed below, where P represents a particle of charge n and S represents a surface with m electrons in its valence band. For the sake of brevity in future discussions, a short-hand notation is introduced for describing each type of transition.

(i) Resonance Transitions

$$P^n + me_S^- \underset{2}{\overset{1}{\rightleftharpoons}} P^{n-1} + (m-1)e_S^-$$

In a *resonant surface-to-particle charge-transfer transition* (S → P) an electron tunnels from a filled level in the solid into a level containing a vacancy at the same energy in the particle. Transition 1 or (S → P) can occur only when the particle possesses a vacancy in the level E_i^v which is within the energy bounds $|E_F| < |E_i^v| < |E_B|$ or $|E_T| < |E_i^v| < |E_B|$.

In a *resonant particle-to-surface charge-transfer transition* (P → S) an electron tunnels from a level of the particle into a vacancy in the solid conduction band at the same energy. Transition 2 or (P → S) can occur only when the particle possesses an occupied level E_i^o which satisfies the condition $|E_i^o| < |E_F|$ and $|E_i^o| < |E_C|$.

(ii) Auger transitions

$$P^n + me_S^- \rightarrow P^{n-1} + (m-2)e_S^- + e^-$$

A *two-electron or Auger surface-to-particle charge-transfer transition* (←S → P) involves the simultaneous transition of two electrons. In such a process an electron from the filled band of the solid tunnels into the particle well and drops into a discrete vacant level; the energy gained is imparted to a second electron of the solid which is excited into the conduction band or ejected into the continuum where it becomes a free electron. Transitions 3 and 3′ or (←S → P) can occur only when the particle possesses a vacancy in the level E_i^v which satisfies the conditions, for a metal, $|E_F| < |E_i^v|$ and, for an insulator, $|E_T| < |E_i^v|$ and $|E_i| \geq |2E_T| - |E_C|$. The so-called "down" (3) and "up" (3′) electrons lose and gain respectively the same amount of energy in this radiationless process. The *Auger particle-to-surface charge-transfer transition* (P → S→) in which an electron from a filled level in the particle drops into the solid valence band and a second valence electron is promoted into the conduction band or continuum can also occur; however, it will occur with a near negligible probability compared to the former (←S → P) process since the solid generally contains no valence band hole into which the "down" electron can fall.

(20) H. D. Hagstrum, *Phys. Rev.*, **96**, 336 (1954); **122**, 83 (1961).
(21) D. V. McCaughan, R. A. Kushner, and V. T. Murphy, *Phys. Rev. Lett.*, **30**, 614 (1973).
(22) D. V. McCaughan and V. T. Murphy, *IEEE Trans. Nucl. Sci.*, **NS-19**, 249 (1972).

Table I. Energetic Requirements and Restraints for Charge-Transfer Transitions Between a Particle and a Surface

	type of transition		
	S → P	P → S	←S → P
metallic surface	$\|E_F\| < \|E_i^v\| < \|E_B\|$	$\|E_i^o\| < \|E_F\|$	$\|E_F\| < \|E_i^v\|$
insulating surface	$\|E_T\| < \|E_i^v\| < \|E_B\|$	$\|E_i^o\| < \|E_C\|$	$\|E_T\| < \|E_i^v\|$
			$\|E_i^v\| \geq \|2E_T - E_C\|$

Hagstrum[19] has calculated the transition probability per unit time, or transition rate $R_t(s)$, as a function of distance s from the surface for (S → P), (P → S), and (←S → P) transitions of rare gas atoms and ions. Values obtained for $R_t(s)$ are of the order of 10^{14} s^{-1} for s = 1–5 Å. The survival probability, $P_o(s,v)$, or the probability that a particle will reach s in its original charge or excitation state or conversely the probability, $P_t(s,v)ds$, that a particle will undergo an electronic transition in the distance element ds at the distance s is strongly dependent on the velocity of the particle. For particles with low velocities such as typical secondary particles whose kinetic energy distributions are maximized below 10 eV (~10^4 m/s), Hagstrum[19] has shown that the survival probability at $s = \infty$ is $P_o(\infty,v) \simeq 0.1$. Hence the probability that a secondary particle will undergo a charge-transfer transition of the type discussed above is extremely high if the transition is energetically feasible and the particle velocity is low. Since typical secondary ion energy distributions[13,14,18] have maxima below 10 eV, charge-exchange transitions in SIMS are the rule rather than the exception. The energetic requirements and restraints for various charge-transfer transitions are summarized in Table I.

III. Experimental Procedures

Details of the design of the SIMS system and pumping facilities have been described elsewhere.[13] The system consists of a stainless-steel ultrahigh vacuum chamber equipped with an Extranuclear Laboratories, Inc., quadrupole mass spectrometer with a "Bessel Box" energy prefilter and a Varian 0–3-keV ion bombardment gun. The SIMS data were acquired by using pulse-counting techniques. A base pressure in the low 10^{-10} torr range was obtained by means of a turbomolecular pump and a titanium sublimation pump. Primary ion bombardment, with the ion gun situated at 60° from the SIMS axis, was performed by backfilling the chamber with He to pressures in the range 1×10^{-8}–1×10^{-6} torr. Under these conditions ion fluxes of 5×10^{-9}–3×10^{-7} A/cm^2 were obtained. Bombardment was performed under dynamic gas-flow conditions, thus providing a continuous stream of fresh He and removing sputtered products. It was necessary to use He gas for bombardment because the heavier rare gases tended to condense on the cold sample. Charging of sample surfaces as a result of ion bombardment was substantial for the molecular solids; compensation was provided by low-energy electrons from an electron flood gun.

The salt samples were reagent grade chemicals and were passed into pellets for analysis. Reagent grade formic acid and nickel tetracarbonyl and distilled, deionized water were frozen on a platinum plate at 77 K for SIMS study. The formic acid and water were degassed by repeated freeze–thaw cycles and introduced into the chamber by means of a tube that directed them to the cold surface.

IV. Results and Discussion

The ejection dynamics and electronic processes occurring during SIMS, as discussed in section II, are applied in this section by classifying materials into four categories: (A) metals, (B) semiconductors, (C) ionic solids, and (D) molecular solids. This classification is mainly for the exemplification of the SIMS features; i.e., most materials can be grouped into one of these categories for the purpose of deciphering their secondary ion patterns.

A. Metals. The work functions of most metals are typically[23] 2–3 eV lower than the ionization potential of the corresponding ground-state metal atom. Hence, there is always an atomic level, E_i^v, which is isoenergetic with a valence band state of the solid, resulting in (S → P) processes for positive ions leaving a metal

(23) "Handbook of Chemistry and Physics", 58th ed., CRC Press, Cleveland, 1977–1978.

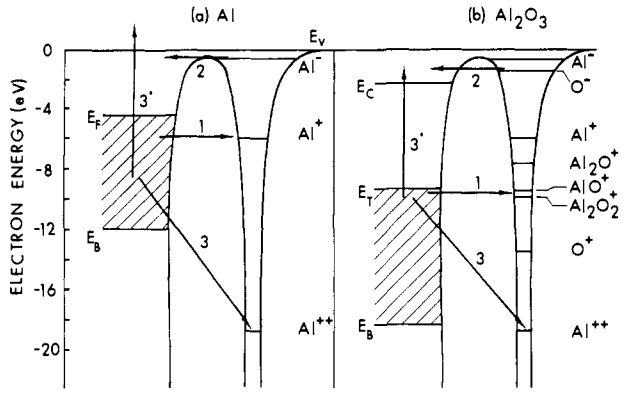

Figure 2. Electron energy diagrams representing secondary particle emission from (a) aluminum and (b) Al_2O_3. The energy levels of several neutral, positive, and negative species are drawn together in the same potential well for convenience.

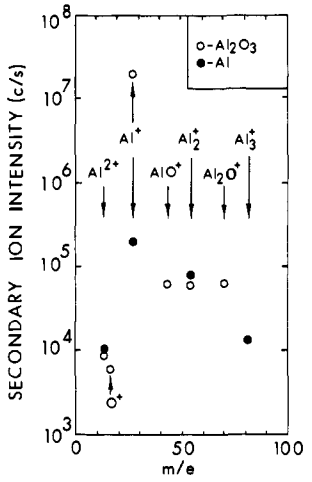

Figure 3. SIMS of positive secondary ions emitted from clean aluminum and Al_2O_3 surfaces. Data are from K. Wittmaack, "Inelastic Ion-Surface Collisions", N. H. Tolk, J. C. Tully, W. Heiland, and C. W. White, Eds., Academic Press, New York, 1977.

surface. Even for cases where $|E_i^v| > |E_B|$, (←S → P) processes can result in neutralization of emerging positive metal ions. The majority of negative ions have electron affinities <1 eV; such species can undergo (P → S) processes by transferring an electron from E_i^o into the conduction band. All this points to the fact that both positive and negative ions can be neutralized by all three of the above processes, resulting in low ion yields from clean metal surfaces. These processes are illustrated in Figure 2a for aluminum metal.

If the metal is oxidized, a band gap develops[24] as shown in Figure 2b for Al_2O_3. From this diagram it is clear that particles emerging as positive ions, for which the vacant level lies in the range E_C to E_T, cannot undergo any kind of neutralizing transition with the surface; hence the initial charge state of the particle as it emerges is preserved at $s = \infty$. Emergent particles such as $Al_2O_2^+$ or O^+ can undergo (S → P) neutralization, Al^{2+} can undergo (←S → P) neutralization, and Al^- and O^- can undergo (P → S) neutralization. Since the species in the oxide lattice already exist in highly polarized states (Al^{3+} and O^{2-}), the initial particles are likely to be ions and will have a high survival probability.

The intensities of the positive SIMS clusters from Al and Al_2O_3 are shown in Figure 3. The Al^+ intensity from the oxide is a factor of 10^2 higher than from the metal due to the lack of neutralization processes in the former. This is a typical result for metal–metal oxide pairs. Al_2O^+ and AlO^+ are observed from the metal oxide with relatively high intensity because they cannot undergo neutralization processes, although AlO^+ lies very close to E_T where the occupied density of metal oxide states is low. Al^{2+} and O^+ have very low intensities due to (←S → P) and (S → P) neutralization processes, respectively. The Al_2^+ intensity from the metal is higher than that from the oxide, and Al_3^+ is not even observed from the oxide; this is due to the fact that Al_n^+ ($n > 1$) clusters from the oxide can only be produced by selvedge reactions since there are no Al nearest neighbors in Al_2O_3. The diagrams of Figure 2 qualitatively account for the intensities of the clusters observed from metal/metal oxide systems. The results for the Al/Al_2O_3 system are typical and apply to most metal/metal oxide systems; the intensity of the atomic ion M^+ from the metal oxide is typically[18] $\sim 10^2$ times greater than that from the clean metal surface.

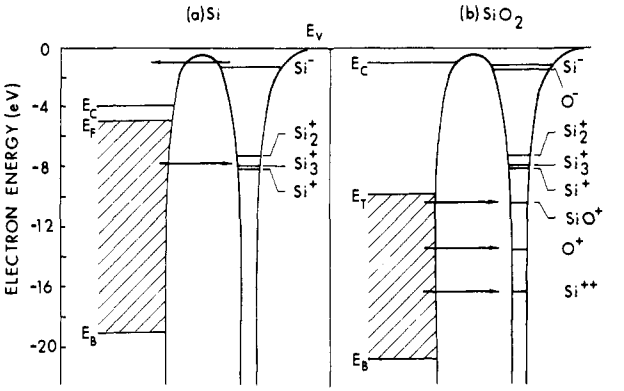

Figure 4. Electron energy diagrams representing secondary particle emission from (a) silicon and (b) SiO_2.

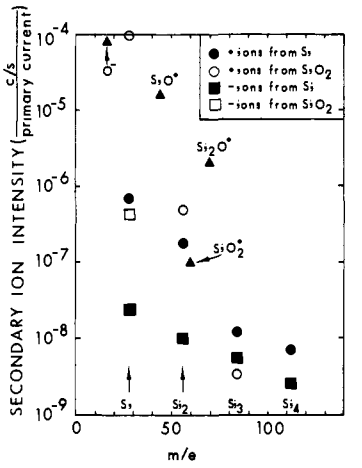

Figure 5. SIMS of positive and negative secondary ions emitted from silicon and SiO_2 surfaces. Data are from K. Whittmaack, "Inelastic Ion-Surface Collisions", N. H. Tolk, J. C. Tully, W. Heiland, and C. W. White, Eds., Academic Press, New York, 1977, and A. Benninghoven, W. Sichtermann, and S. Storp, *Thin Solid Films*, **28**, 59 (1975).

B. Semiconductors. As an example of sputtering from a semiconductor, we consider silicon[25] and the energy levels of its various secondary particles in Figure 4a. Emerging positive ions can undergo (S → P) and (←S → P) transitions while negative ions can undergo (P → S) transitions. Since the atoms are covalently bound in the solid, they will emerge from the solid predominantly as neutral species and such neutral species cannot undergo (P → S) transitions to yield positive ions because the valence band of Si is filled. As a result, clean Si has a low ion yield similar to clean metals.

The diagram for SiO_2 (Figure 4b) shows that the large band gap[21] makes it impossible for emerging Si^+, Si_2^+, Si_3^+, Si^-, and O^- to undergo any charge-exchange processes with the surface. Since the SiO_2 lattice consists of positive silicon and negative

(24) A. Bianconi, R. J. Bachrach, S. B. M. Hagstrom, and S. A. Flodström, *Phys. Rev. B*, **19**, 2837 (1979).

(25) J. A. Taylor, G. M. Lancaster, A. Ignatiev, and J. W. Rabalais, *J. Chem. Phys.* **68**, 1776 (1978).

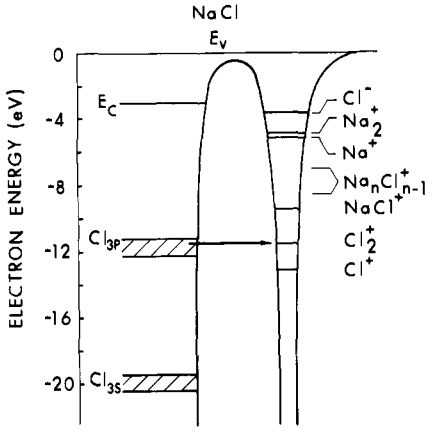

Figure 6. Electron energy diagram representing secondary particle emission from NaCl.

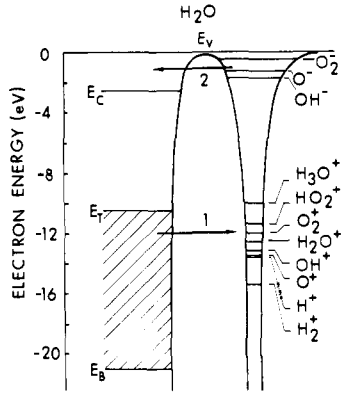

Figure 7. Electron energy diagram representing secondary particle emission from ice at 77 K.

oxygen ions, the particles will be sputtered predominantly as charged entities. As a result, SiO_2 has a high ion yield.

The intensities of positive and negative SIMS clusters from Si and SiO_2 are shown in Figure 5. Note that the ratio Si_n^+(oxide)/Si_n^+(semiconductor) for n = 1, 2, and 3 is 143, 2.7, and 0.28. The high ratio for n = 1 is expected from the above discussion. The drastic decrease in the ratio for n = 2 and 3 is due to the fact that collisions in the selvedge are necessary to produce Si_2^+ and Si_3^+ from SiO_2 but not from Si. Hence, even though Si_3^+ can be (S → P) neutralized near the Si surface, the fact that it can result from nonreactive ejection renders it more abundant than its counterpart from SiO_2, where collisions are necessary to form the species although, once formed, it survives to $s = \infty$. The ratio Si^-(oxide)/Si^-(semiconductor) is high, as in the positive ion case, due to the inability to neutralize Si^- at the SiO_2 surface. Although Si_n^- clusters with n = 2, 3, and 4 are observed from Si, their intensities from SiO_2 are so low that they do not appear on the figure. This is largely due to the selvedge collisions required for n = 2, 3, and 4 cluster production from SiO_2. Note that although O^- from SiO_2 is very intense (it cannot be (P → S) neutralized), O^+ is too weak to appear on the chart (emerging O^+ can be (S → P) neutralized and emerging O remains neutral). SiO^+ is very intense because the ionization potential of SiO is near E_T where the density of occupied states is very low,[26] resulting in a low (S → P) transition probability. The high Si_2O^+/SiO_2^+ ratio is due to the fact that the ionization potentials of the neutral silicon oxides vary as Si_2O < SiO < SiO_2; this places Si_2O^+ in a region where (S → P) processes are energetically forbidden and SiO_2^+ in a region where such processes are highly probable.

C. Ionic Solids. The band structure[26-28] of NaCl is shown in Figure 6 as representative of an ionic solid; such species have narrow valence bands with large gaps between them. Of the atomic and molecular ionization energies[29] indicated in the potential well, only emerging Cl_2^+ and Cl^+ can be neutralized; the process is a resonant (S → P) transition. All other species leaving in the form of positive or negative ions cannot be neutralized because the vacant levels of the ion lie in the broad band gaps and Auger processes are energetically not feasible. SIMS for such salts exhibit very high ion yields since the species already exist as ions in the solid, i.e., Na^+ and Cl^-, and they cannot be neutralized by the surface.

The SIMS[13] of such MX salts all exhibit ions of the type M^+, M_2^+, MX^+, M_nX_{n-1} (n = 2, 3, ..., 11), and X^- with high intensity. The $M_nX_{n-1}^+$ series dominates the spectrum, extending, for example, to n = 14 in NaF, with intensities given by the expression $I = aM^b$ where I is the observed cluster intensity (counts/s), M is the cluster mass, and a and b are constants whose values are typically, for NaCl, 1.4×10^{17} and −5.77, respectively. The secondary ion energy distributions[13] of M^+ and M_2^+ ions are maximized at somewhat higher energies than those of the $M_nX_{n-1}^+$ clusters, suggesting that the former result from direct nonreactive ejection while the latter are produced by ion attachment reactions in the selvedge. The $M_nX_{n-1}^+$ clusters consisting of a single M^+ ion surrounded by MX species are very stable; although the ionization energies of the corresponding neutral clusters are not known, they will certainly be less than that of NaCl, placing them in the band gap where they cannot be neutralized. The intensity ratio $Na_2Cl^+/NaCl^+$ is $\sim 10^2$, suggesting that $NaCl^+$ is not extremely stable, tending to decompose to yield the species Na^+ and Cl or to attach itself to other moities in the selvedge.

D. Molecular Solids. The composition of SIMS clusters emitted from molecular solids, while governed by all of the processes discussed in section II, are modified by the existence of strong bonds between the atoms of a molecule. The different bond strengths between specific atom pairs are largely responsible for the fragmentation patterns observed in gas-phase mass spectrometry; likewise in SIMS, such patterns can be related to the bonding and molecular structure existing on a surface. While it is possible to derive information about surface bonding and structure from SIMS, it is important to recognize that some clusters may come from rearrangement or attachment reactions and may not be representative of the virgin surface structure. While this model cannot account for all of the ions observed from complex molecular solids, it is consistent with the qualitative relative abundances of the secondary ions when the energy levels of these ions are compared to those of the parent solid compound. The discussion of molecular solids is facilitated by division into two subgroups: *those with* (1) *strong intermolecular forces and* (2) *strong intramolecular forces*. We consider examples in both of these categories.

(1) Molecular Solids with Strong Intermolecular Forces. Ice is an excellent example of this category due to its strong intermolecular hydrogen bonds. The band structure[30,31] of ice and the ionization potentials of several species that could be ejected from the surface are depicted in Figure 7. From this diagram we see that all emerging negative ions can undergo (P → S) neutralization and all positive ions, with the exception of H_3O^+, can undergo (S → P) neutralization. Auger processes are not possible due to the large band gap. The positive SIMS[14] of ice is dominated by a long series of the type $H(H_2O)_n^+$ (n = 1, 2, ..., 51). All neutral $H(H_2O)_n$ clusters with $n > 1$ will have smaller ionization energies than H_3O which will locate them in the gap between E_C and E_T; H_3O itself is close to E_T where the density of states is small and some (S → P) processes may be possible. The secondary ion energy distributions[14] suggest that H_3O^+ is produced by nonreactive ejection while the larger clusters ($n > 1$) are produced

(26) T. Ohta, S. Kinoshita, and H. Kuroda, *J. Electron Spectrosc. Relat. Phenom.*, **12**, 169 (1977).
(27) R. T. Poole, J. G. Jenkin, J. Liesegang, and R. C. G. Leckey, *Phys. Rev. B*, **11**, 320 (1975).
(28) W. A. Harrison, "Electron Structure and the Electronic Properties of Solids", W. H. Freeman, San Francisco, Calif, 1980, p 321.
(29) W. C. Price, "Electron Spectroscopy", Vol. 1, C. R. Brundle and A. D. Baker, Eds., Academic Press, New York, 1977, p 178.
(30) M. J. Campbell, J. Liesegang, J. D. Riley, R. C. G. Leckcy, and J. G. Jenkin, *J. Electron Spectrosc. Relat. Phenom.*, **15**, 83 (1979).
(31) R. Onaka and T. Takahashi, *J. Phys. Soc. Jpn.*, **24**, 548 (1968).

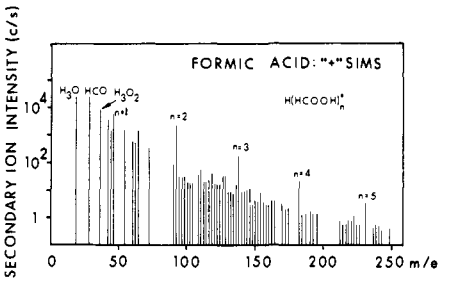

Figure 8. Positive SIMS of formic acid frozen at 77 K by using He^+ primary ions.

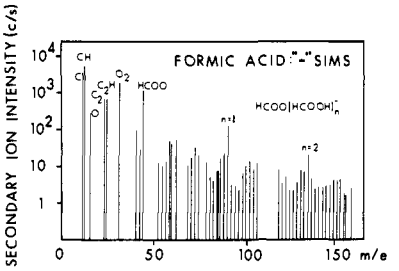

Figure 9. Negative SIMS of formic acid frozen at 77 K by using He^+ primary ions.

by attachment reactions. This would suggest that the H_3O^+ intensity should be much higher than that of the $n > 1$ clusters. That is not the case—$H(H_2O)_4^+$ representing a symmetrical H_3O^+ ion surrounded trigonally by three H_2O molecules is the most abundant ion.[14] This apparent anomaly is most likely due to the fact that the ionization potential[32] of H_3O is close to E_T so that some (S → P) neutralization of emerging H_3O^+ occurs, whereas the transition is energetically forbidden for the $n > 1$ clusters whose neutral counterparts have smaller ionization potentials. The observation[14] of such a long series of cluster ions is indicative of the efficacy of the clustering process during expansion through the selvedge. The negative SIMS of ice exhibits only small ions (any large negative clusters are of very low intensity) whose abundances are low compared to the positive ions.

As another example of a molecular solid with strong intermolecular hydrogen bonding, the positive and negative SIMS of frozen formic acid are presented in Figures 8 and 9. Although the band structure of solid formic acid is not known, a diagram similar to Figure 7 would be expected to result in this case. The spectra are dominated by series of the type $H(HCOOH)_n^+$ and $HCOO(HCOOH)_n^-$ as well as fragment clusters and are a good example of a case in which all three dynamical sputtering processes are operative. Nonreactive ejection would account for the $HCOOH^+$ and $HCOOH^-$ ions as well as some of the intensity of the ions HCO^+, C^-, and CH^-. Attachment and rearrangement reactions produce the cluster series with $n = 2$, 3, 4, and 5 as well as species such as H_3O^+, $H_3O_2^+$, C_2^-, C_2H^-, and O_2^-. Fragmentation processes may be responsible for the intermediate species observed between the $n = 1, 2, \ldots$, and 5 series and some of the intensity of the smaller ions such as HCO^+, C^-, and CH^-.

(2) Molecular Solids with Strong Intramolecular Forces. The positive SIMS of frozen nickel tetracarbonyl is shown in Figure 10 as an example of a molecular solid with strong intramolecular bonds and only van der Waals forces between the condensed molecules. Although the position of E_T for solid $Ni(CO)_4$ is not known, the ionization potential[33] of the free $Ni(CO)_4$ molecule at ~8.6 eV is certainly higher than E_T (this is the case for all other transition-metal carbonyl compounds for which the data[34] are available). An emerging parent molecular ion can then be

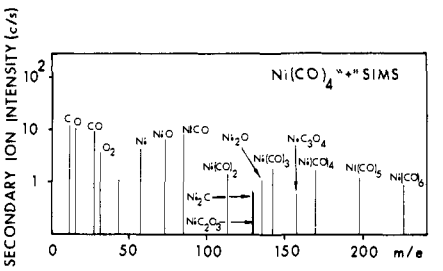

Figure 10. Positive SIMS of nickel tetracarbonyl frozen at 77 K by using He^+ primary ions.

neutralized by a (S → P) process since the solid compounds have fairly broad band structures. Since the molecules are covalently bonded in the solid, neutral species should be ejected in highest abundance and these neutrals will survive, resulting in very low ion yields from such materials. The SIMS[14] of frozen benzene and cyclohexane provide similar low ion yields.

The positive SIMS of $Ni(CO)_4$ exhibits clusters from all three dynamical sputtering processes. Nonreactive ejection produces $Ni(CO)_4^+$ and may be responsible for some of the intensity of species such as C^+, O^+, CO^+, O_2^+, Ni^+, $NiCO^+$, $Ni(CO)_2^+$, and $Ni(CO)_3^+$. Rearrangement and attachment reactions in the selvedge produce $Ni(CO)_5^+$, $Ni(CO)_6^+$, CO_2^+, NiO^+, Ni_2C^+, Ni_2O^+, $NiC_2O_3^+$, and $NiC_3O_4^+$. Decomposition of the parent ion can also produce some of the intensity of the fragment clusters. An approximate indication of the types of fragments originating from molecular decomposition of the parent can be obtained from the gas-phase mass spectrum of $Ni(CO)_4$; comparison with the SIMS intensities of the fragments shows that nonreactive ejection accounts for a large portion of the fragment intensity.

SIMS has been applied[6-8] with success to the study of chemisorbed molecules on metal surfaces in order to determine the nature of the adsorbed species and adsorption bonds. Success in such studies has usually come from studying the variation of specific cluster intensities as a function of adsorbate coverage. However, the mere observation of a specific cluster from an adsorbate/substrate system is not necessarily absolute proof of the existence of that species on the virgin surface. An example is the adsorption of CO on Ni, where the observation[35] of Ni_2CO^+ clusters in the SIMS was taken as evidence for bridged CO bonding on the surface atoms. The clusters Ni_2C^+ and Ni_2O^+ are observed in the SIMS of $Ni(CO)_4$ where there are no adjacent Ni atoms.

SIMS has been used[9-12] as an ionization source for nonvolatile, thermally labile organic compounds whereby the parent molecule can be detected in its cationized form. In cationization,[1] a molecule R is attached during the sputtering process to a metal ion M^+ from the metallic substrate upon which the compound is deposited and the resulting adduct $(RM)^+$ is detected. The process can occur by means of a selvedge reaction between molecules R and ions M^+; it can also occur by nonreactive ejection in cases where the RM bond is very strong and $(RM)^+$ can be sputtered by breaking the weaker metal–metal bonds. It has been shown that such cationization and anionization are the dominant processes occurring for many large molecules with polar groups (such as amino acids and peptides) where strong RM bonds are expected. For these compounds the dominant clusters are "parent-like" ions of the type $(RM)^+$, $(RH)^+$, and $(R-H)^-$ with low fragment ion abundance. Cationization and its analogue, anionization, are observed in the SIMS of ice[14] and formic acid (Figures 8 and 9) where H^+ is the adduct rather than metal ions. The long series of clusters $M_nX_{n-1}^+$ observed[13] from ionic salts, section IV. C, can also be considered as cationized molecules.

V. Conclusions

The qualitative model presented here is consistent with the types of secondary particles observed in SIMS and their relative

(32) A lower limit to the ionization potential of H_3O, $E_i(H_3O, \text{low})$, can be obtained from the enthalpies of formation of the appropriate species; i.e., $E_i(H_3O, \text{low}) = [\Delta H^f(H_3O^+)] - [\Delta H^f(H) + \Delta H^f(H_2O)] = 10.4$ eV.

(33) J. H. D. Eland, "Photoelectron Spectroscopy", Halsted Press, New York, 1974.

(34) E. W. Plummer, W. R. Salaneck, and J. S. Miller, *Phys. Rev. B*, **18**, 1673 (1978).

(35) M. Barber, J. C. Vickerman, and J. Wolstenholme, *J. Chem. Soc., Faraday Trans.*, **172**, 40 (1976).

abundances for a variety of materials. The treatment decomposes secondary particle emission into two steps, i.e., ejection dynamics and electronic processes. Ejection dynamics in the selvedge govern the types of particles emitted and their atomic composition and cluster size. The origins of the particles can be traced to three dynamical processes: (i) nonreactive ejection, (ii) reactions in the selvedge, and (iii) fragmentation of clusters. Particles are emitted predominantly in the same charge state in which they exist in the material. These charge states can be modified while the emerging particle is within a few angstroms of the surface by particle–surface electronic charge-transfer transitions of the resonance or Auger type. *Emerging positive ions have a high probability of being neutralized by resonance surface-to-particle ($S \rightarrow P$) or Auger surface-to-particle ($\leftarrow S \rightarrow P$) charge-transfer transitions if the resulting neutral particle ionization potential (or vacant level in the positive ion, E_i^v) is below the Fermi level or top of the valence band of the solid. Emerging negative ions have a high probability of being neutralized by resonance particle-to-surface ($P \rightarrow S$) charge-transfer transitions if the electron affinity of the resulting neutral particle (or an occupied level of the negative ion, E_i^o) is quasi-degenerate with a vacancy in the conduction band of the solid.* The highest secondary ion yields are obtained from materials with large bands and narrow valence bands where these charge-exchange processes are improbable and the lowest ion yields are obtained from clean metals where charge-exchange processes dominate due to the broad bands. The model correctly accounts for the cluster types and their qualitative abundances observed in SIMS of metals, metal oxides, ionic salts, binary solids, and very simple molecular solids; however, as molecular size and complexity increase, the ability of the model to account for the multitudes of fragments and clusters rapidly decreases. The model is therefore proffered as a means of rationalizing and correlating SIMS results for the classes of materials described above.

Acknowledgment. This material is based upon work supported by the National Science Foundation under Grant No. CHE-7915177. We thank S. S. Ni for assistance with the SIMS of solid HCOOH and $Ni(CO)_4$.

Reversed Micelles of Aerosol-OT in Benzene. 2. Equilibrium Studies Using Vapor Pressure Osmometry and Spectrophotometry with Picric Acid as Indicator[1,2]

Kiyoshi Tamura[3] and Z. A. Schelly*

Contribution from the Department of Chemistry, The University of Texas at Arlington, Arlington, Texas 76019. *Received June 23, 1980*

Abstract: Vapor pressure osmometric results on Aerosol-OT (AOT) in benzene (with 0.03% w/w water) can best be interpreted in terms of either an empirical description or a bimodal equilibrium model. The empirical description yields only a single type of reversed micelle with mean aggregation number of $\bar{n} = 11.6$ at 25 °C and a constant monomer concentration $[A]_o = 4 \times 10^{-4}$ M at surfactant concentrations $C_{AOT} \geq 10^{-2}$ M. $[A]_o$ may be regarded as the operational cmc of the system. The bimodal model describes aggregation by association equilibria in which a discrete monomer–6-mer–14-mer system is formed where the concentration of all species present increases with C_{AOT}. The concept of cmc is absent from this model. Spectrophotometric studies of the solubilization of picric acid indicator by AOT reversed micelle indicate that either of the two equilibrium models can serve the quantitative description of the solubilization if only a small fraction α of the micelles is eligible to accommodate picric acid in their polar interior. The solubilization equilibria lead formally to equations which suggest that the solubilization process can be regarded as adsorption of the indicator by the micelle. Numerical values of the formation constants, solubilization constants, and the α's are reported.

In a recent communication,[1] we reported preliminary concentration-jump kinetic results on the rate of solubilization of picric acid by reversed micelle of Aerosol-OT (AOT, bis(2-ethylhexyl) sodium sulfosuccinate) in benzene containing 0.03% w/w water. The faster of the two distinct rate processes observed in the millisecond range was interpreted by a two-step penetration mechanism, and the slower one was tentatively related to substrate-induced micelle formation or to the reconstruction of the indicator-containing micelles.

For the further elucidation of the mechanism of solubilization, it was necessary to obtain additional information about the physical meaning of the critical micelle concentration (cmc) for this system, the state of aggregation of AOT, and the effect of the probe molecule on the micelle formation, as well as information about the states of the picric acid probe existing in the surfactant solution.

In the present work, we report vapor pressure osmometric and spectrophotometric results on the reversed micelle of AOT in benzene, obtained in or without the presence of picric acid as indicator. The results of computer analysis of the equilibrium data are presented. The equilibrium characterization of the AOT–benzene system thus obtained is utilized in the detailed kinetic analysis of the solubilization of picric acid, described in the companion paper.[2]

Experimental Section

Chemicals. Aerosol-OT (Pflatz & Bauer, Inc.) and the solvent benzene were purified as described previously.[4] The dry benzene contains 0.03% w/w of water.[4] Picric acid (Eastman Kodak Co.) was recrystallized three times from water and dried under vacuum. All other reagents used were of reagent grade.

Spectrophotometric Measurements. The absorption spectra in the wavelength range of 280–600 nm were recorded on a Cary 219 spectrophotometer equipped with automatic base-line correction. Quartz cells of 1-cm path length were used in all experiments, thermostated at 25 °C.

Vapor Pressure Osmometry. A Hewlett-Packard Model 302B vapor pressure osmometer equipped with a variable-temperature controller was used. The instrumental calibration procedure and the method of measurements were similar to those described previously.[4] For temperature equilibration, each sample was kept in the syringe for at least 10 min

(1) Part 1 of this series: Tamura, K.; Schelly, Z. A. *J. Am. Chem. Soc.* **1979**, *101*, 7643–7644.
(2) Part 3: Tamura, K.; Schelly, Z. A. *J. Am. Chem. Soc.*, following article in this issue.
(3) R. A. Welch Postdoctoral Fellow. On leave of absence from the National Defense Academy, Yokosuka, Japan.
(4) Herrmann, U.; Schelly, Z. A. *J. Am. Chem. Soc.* **1979**, *101*, 2665–2669.

0002-7863/81/1503-1013$01.25/0